

Non-equilibrium dynamics of an active colloidal “chucker”

C. Valeriani,^{*} R. J. Allen,[†] and D. Marenduzzo[†]

*SUPA, School of Physics and Astronomy, University of Edinburgh,
Mayfield Road, Edinburgh, EH9 3JZ, Scotland*

Abstract

We report Monte Carlo simulations of the dynamics of a “chucker”: a colloidal particle which emits smaller solute particles from its surface, isotropically and at a constant rate k_c . We find that the diffusion constant of the chucker increases for small k_c , as recently predicted theoretically. At large k_c the chucker diffuses more slowly due to crowding effects. We compare our simulation results to those of a “point particle” Langevin dynamics scheme in which the solute concentration field is calculated analytically, and in which hydrodynamic effects arising from colloid-solvent surface interactions can be accounted for in a coarse-grained way. By simulating the dragging of a chucker, we obtain an estimate of its apparent mobility coefficient which violates the fluctuation-dissipation theorem. We also characterise the probability density profile for a chucker which sediments onto a surface which either repels or absorbs the solute particles, and find that the steady state distributions are very different in the two cases. Our simulations are inspired by the biological example of exopolysaccharide-producing bacteria, as well as by recent experimental, simulation and theoretical work on phoretic colloidal “swimmers”.

^{*}Author to whom correspondence should be addressed. Electronic addresses: cvaleria@ph.ed.ac.uk

[†]RJA and DM made an equal contribution to this work

I. INTRODUCTION

Understanding the properties of colloidal systems which are intrinsically out-of-equilibrium as they are active, is an important emerging goal in soft matter physics, driven both by the potential for modelling motile cells as active colloidal “swimmers”, and for designing self-propelled particles with novel nanotechnological applications [1–7]. Several mechanisms for colloidal self-propulsion have been proposed: these can be broadly grouped into those where the colloid exerts force on the surrounding fluid (as for swimming bacteria or other motile cells) [1–5], and those in which the colloid changes the chemical properties of the surrounding medium in an asymmetric way by catalysing a chemical reaction on its surface [8–10] or by secreting some product [11–15].

In this paper, we consider a “chucker”: a spherical colloidal particle which produces smaller “solute” particles at its surface. Our model colloid is simpler than most cases considered thus far [12–15], since it “chucks” solute particles isotropically, and therefore does not display directional motion. However, the chucking drives our system out of equilibrium, giving it interesting dynamical properties. We find that the effective diffusion constant of the chucker increases with the chucking rate k_c for low k_c , and eventually decreases for high k_c due to self-crowding. We further simulate the dragging of a chucker, to obtain a measurement of its effective mobility. Comparing this to the effective diffusion constant allows us to show that the fluctuation-dissipation theorem does not hold in this non-equilibrium system, and that the deviations from the FDT are non-monotonic in the chucking rate. Finally, we consider the steady-state positional probability distribution function for a chucker which sediments against a planar surface, in the case where the surface is “hard”, and in the case where the surface absorbs the solute particles.

Although our model is designed to be generic, our work is inspired by the observation that many bacterial cells secrete extracellular polysaccharides [16, 17], in some cases in large quantities (for example the bacterium *Xanthomonas campestris* can produce xanthan polymer at a rate as high as 10^4 polymer molecules per cell per second [18, 19]). These exopolysaccharides can have important effects on the collective properties (e.g. phase behaviour) of assemblies of bacteria [20]. Our simulations suggest that in some cases exopolysaccharide production might also affect the diffusive motion of single bacterial cells. We note that the case of a chucker sedimenting onto an absorbing surface might be relevant

to exopolysaccharide-producing bacteria located close to a biofilm.

Several recent works have considered the dynamics of colloids which produce surface particles from a theoretical point of view [12–15, 21] and using simulations [13]. The key concept here is that motion of the colloid can be generated by a concentration gradient of solute, produced by the colloid itself. Most previous work has considered the case where the colloid produces solute anisotropically across its surface, resulting in directional motion. In contrast, we consider the case where solute is produced isotropically, so that the solute concentration gradient is on average symmetrical about the colloid. However, as we show here, solute production nevertheless has a strong effect on the dynamical fluctuations of the colloid. The case of an isotropic chucker has recently been considered theoretically by Golestanian [11]. Using scaling theory and linearised hydrodynamics, he predicts inertial and diffusive dynamical regimes, separated by an anomalous regime for intermediate timescales in which the mean square displacement scales as the $3/2$ power of time. He further predicts that in the diffusive regime, the effective diffusion constant scales linearly with the chugging rate. In this paper, we test these predictions using numerical simulations.

The question of how a solute concentration gradient influences colloid motion has some subtleties. From one point of view, both the colloid and the solute particles are large compared to the solvent particles; Brownian Dynamics (BD) simulations, in which the solvent is replaced by a stochastic force on the particles, are generally believed to work well in this regime [22–25]. In such a BD representation, a concentration difference of solute across the colloid surface would produce a force on the colloid $\mathbf{f} = -k_B T \int \hat{\mathbf{n}} c dS$ where c is the local concentration of solute, the integral is over the colloid surface, $\hat{\mathbf{n}}$ is the normal to the surface, k_B is the Boltzmann constant and T is the temperature [13]. However, such a BD representation does not take account of the details of the solvent motion close to the chucker surface. This may be important, since, as emphasised recently by Jülicher and Prost [21], hydrodynamic theory using linearised non-equilibrium thermodynamics predicts that relative motion between the colloid and solvent is dependent on the existence of a surface slip velocity. In a simple view, the density of the solvent is expected rapidly to compensate any imbalances in the solute concentration field to maintain a constant overall isotropic pressure, except in a very narrow region around the colloid where molecular interactions between the colloid surface and the solute can generate a surface slip velocity. Equivalently, one might state that in order to generate a force, the configuration of solute particles relative to the

colloid surface must change when the colloid moves. Because the solute moves with the fluid, such a configurational change can only be achieved if there is a surface slip velocity.

As discussed by Golestanian *et al* [11, 12], the colloid velocity can be expressed as the integral over the colloid surface of a slip velocity $\mathbf{v}_s = -\mu\nabla c$ where c is the solute concentration, μ the surface mobility $\mu = k_B T \lambda^2 / \eta$, η being the viscosity and λ a length-scale. In the non-permeable case, the latter is the Derjaguin length, describing the range of interactions between the colloid and solute. The length-scale λ is then small, so that the linearised theory predicts that chucker will have little effect on colloidal motion. However, Adjari and Bocquet [26] have shown recently that for solutes smaller than the intrinsic slip length, a small degree of surface slip can lead to large enhancements of λ . Moreover, for colloids that are partially or fully permeable to solvent (osmiophoresis), anything between this result and a much larger colloid velocity, equal to the “naive” kinetic force $\mathbf{f} = -k_B T \int \hat{\mathbf{n}} c dS$ multiplied by a mobility factor, is possible [12, 27]. The motion of a semi-permeable rigid vesicle in response to a solute gradient has been analysed in a linearised framework by Anderson [28]. In a later work, the applicability of the linearised theory to this type of problem has been called into question by an experimental study by Nardi *et al* [27]. These authors measured the motion of lipid vesicles in a solute concentration gradient, and found a drift velocity more than 3 orders of magnitude faster than that predicted by the linearised theory, suggesting that a strong nonlinear coupling exists between osmosis and hydrodynamic flow.

Our simulations do not include explicit solvent particles. Instead, we model the chucker as a diffusing hard sphere and the solute particles as diffusing hard spheres which interact only with the chucker. We use a dynamical Monte Carlo (MC) simulation scheme which has been shown to be equivalent to Brownian Dynamics for small trial displacements [22–25, 29]. By simulating a passive colloid in a fixed gradient of solute particles, we show that the naive kinetic result for the colloid velocity, expected for Brownian Dynamics simulations, is recovered in our MC simulations, at least for small solute particles. To estimate the likely effects of neglecting the detailed solvent-chucker interactions, we complement our MC simulations with a Langevin dynamics approach, in which the chucker is modelled by a diffusing point particle which experiences a drift force proportional to the local solute concentration gradient. The prefactor linking the force to the density gradient (which is proportional to λ) can be varied, mimicking the effects that would be expected with explicit solvent. The Langevin simulations are in qualitative agreement with our MC results; this

agreement is also quantitative, for suitably chosen λ , for low chucking rates and when the solute particles are small compared to the colloid.

This work is structured as follows. In the next Section, we describe in detail our simulation model and methods. In Section III we report results for a diffusing chucker, a dragged chucker and a chucker close to a surface. Finally, Section IV contains a discussion and our conclusions.

II. MODEL AND METHODS

We model the chucker as a hard sphere of radius R_1 , with long-time diffusion coefficient D_1 . With a rate k_c , the sphere produces (“chucks”) smaller particles (solute) isotropically at its surface. The solute particles have radius R_2 and long-time diffusion coefficient D_2 , which is related to D_1 by Stokes’ law: $D_2/D_1 = R_1/R_2$.

In our simulations, the length unit is the chucker radius R_1 and we use two different values for the solute radius R_2 : $R_2/R_1 = 0.1$ ($R_1/R_2 = 10$) or $R_2/R_1 = 0.01$ ($R_1/R_2 = 100$).

A. Monte Carlo simulations

Our main simulation results are obtained using a dynamical Monte Carlo algorithm. In this algorithm, a particle is chosen at random and subjected to a trial displacement δ , in a randomly chosen direction and with magnitude uniformly distributed in the range $0 \rightarrow 0.001R_1$ (for the chucker) and $0 \rightarrow 0.001R_1\sqrt{R_1/R_2}$ for the solute particles (this ratio of displacements is to ensure the correct ratio between the diffusion coefficients D_1 and D_2 , as given by Stokes’ Law). If this trial displacement results in an overlap between chucker and solute, it is rejected; otherwise it is accepted. One MC cycle consists of N trial displacements, where N is the current number of particles in the system. It has been shown in previous literature [22–25, 28–30] that this algorithm is equivalent to Brownian Dynamics for small trial displacements. An MC cycle can be interpreted as the time unit in a dynamical trajectory, where the diffusion constant in reduced length units is given by $D_1/R_1^2 = \frac{(\delta R_1/R_1)^2}{6}$ [MC cycles] $^{-1}$. At the beginning of every MC cycle, a new solute particle is inserted with uniform probability of k_c , randomly at the surface of the chucker. Note that because the solutes do not interact, all particle insertions are accepted. All values for

the chucking rate k_c in our MC simulations are in units of [MC cycles] $^{-1}$. This dynamical MC scheme allows us to represent the solute particles as penetrable hard spheres and easily to insert new solute particles, both of which would be difficult in a standard Brownian Dynamics scheme.

The chucker and the solute particles interact according to the Asakura-Oosawa-Vrij (or penetrable hard sphere) model [31–33]: the solute particles cannot overlap with the chucker but do not interact with each other:

$$\begin{aligned}
 v_{ss} &= 0 \\
 v_{sc} &= 0 && \text{if } r_{sc} > R_1 + R_2 \\
 v_{sc} &= \infty && \text{if } r_{sc} \leq R_1 + R_2
 \end{aligned}
 \tag{1}$$

where v_{ss} and v_{sc} are the solute-solute and solute-chucker interaction energies, and r_{sc} is the distance between the centres of the solute and chucker particles.

Figure 1 shows snapshots from our MC simulations. To prevent the number of solute particles from growing indefinitely during the simulations, solutes need to be removed at some large distance from the chucker. Our system reaches a steady state when the rate of solute particle generation at the chucker surface equals the rate of solute absorption at the boundary. We achieve this in two different ways. For simulations with a fixed wall (as shown in the right-hand panel of Figure 1), we define a fixed cubic simulation box and remove any solute particles which stray outside this box. For simulations in the bulk (as shown in the left panel of Figure 1), we remove any solute particles that stray outside a cubic box with sides of length $2L$, centred on the current position of the chucker. The box size is large enough to have no effect on the results reported here ($L = 6R_1$). We have also verified that for our parameter set, the results are independent of the box size. Figure 2 shows the steady-state concentration profile of solute particles around the (moving) chucker, for several different values of L : for $L \geq 6R_1$, the solute concentration profile is virtually independent of L .

B. Langevin Dynamics simulations

To facilitate the simulation of larger systems, and to better understand the underlying physics, we have also simulated our system using an overdamped Langevin dynamics algo-

rithm [34], in which the chucker is represented as a point particle and the solute particles are represented as a space and time-dependent density field, the gradient of which provides a force on the chucker. In a mean-field approach, we assume that the density of solute particles can be obtained from the time-dependent analytical solution of the free-space diffusion equation with a point source (the chucker), integrated over the previous trajectory of the chucker. This approach assumes that the thermal fluctuations of the chucker are slower with respect to the solute diffusion, and further neglects thermal fluctuations in the solute density. A similar approach has recently been used to simulate a microorganism performing chemotaxis by Sengupta *et al* [7].

In our Langevin dynamics simulations, the force \mathbf{f} on the “point chucker” depends on the concentration profile $c(\mathbf{r})$ of the solute according to [12, 28, 30, 35]:

$$\mathbf{f} = -A\nabla c(\mathbf{r}) \quad (2)$$

where the prefactor A is determined by the physical process by which an osmotic pressure gradient is converted into colloidal motion. This force produces a drift velocity \mathbf{v} which is related to the force \mathbf{f} by $\mathbf{f} = k_B T \mathbf{v} / D_1 = 6\pi\eta R_1 \mathbf{v}$. By tuning the prefactor A , we can tune the drift velocity \mathbf{v} . If the solvent-chucker interactions were to be properly taken into account, linearised theory suggests that the drift velocity would be given by Golestanian’s relation $\mathbf{v}_s = -k_B T \lambda^2 \nabla c / \eta$ [11], where (as discussed earlier) λ is related to the lengthscale of solvent-colloid interactions. By combining this relation with Eq.(2), we can obtain an “effective” value of λ for our Langevin dynamics simulations: $\lambda = \sqrt{A / (6\pi R_1 k_B T)}$. A full treatment, including solvent, with this value of λ , would give the same drift velocity as our Langevin dynamics simulations with prefactor A . By varying the prefactor A , we can vary the effective λ value. By choosing λ values corresponding to realistic solvent-colloid interaction lengths, we should obtain results closer to those that would be expected for a full treatment including solvent. In contrast, in our Monte Carlo simulations, the value of λ is fixed. Here, the net force on the chucker produced by the imbalance of solute collisions across the colloid surface [13] corresponds to a value $A = (4/3)\pi R_1^3 k_B T$, or alternatively an effective $\lambda = \sqrt{2} R_1 / 3$.

The concentration profile $c(\mathbf{r})$ is not represented explicitly in our simulations but is calculated analytically from the time history of the position of the point chucker:

$$c(\mathbf{r}) = k_c \int_0^t dt' G(\mathbf{r} - \mathbf{r}', t - t'), \quad (3)$$

where $\mathbf{r} \equiv \mathbf{r}(\mathbf{t})$, $\mathbf{r}' \equiv \mathbf{r}(\mathbf{t}')$ and $G(\mathbf{r} - \mathbf{r}', t - t')$ is the Green's function for the diffusion equation in free space with a sink at infinity (valid for comparison to our MC simulations when the MC boundary position L is large):

$$G(\mathbf{r} - \mathbf{r}', t - t') = \frac{1}{8(\pi D_2(t - t'))^{3/2}} \exp \left[-\frac{(x - x')^2 + (y - y')^2 + (z - z')^2}{4D_2(t - t')} \right] \quad (4)$$

where D_2 is the diffusion constant for the solute. We now define $F(\mathbf{r} - \mathbf{r}', t - t') = \nabla G(\mathbf{r} - \mathbf{r}', t - t')$. Since in our Langevin dynamics algorithm the particle moves in discrete steps, we can replace the integral in Eq.(3) by a sum of $F(\mathbf{r} - \mathbf{r}', t - t')$ over the previous trajectory of the particle, giving us a history-dependent expression for the force on the particle:

$$\mathbf{f}(t) = -Ak_c \sum_{i=1}^M \Delta t F(\mathbf{r}(t) - \mathbf{r}(t - i\Delta t), i\Delta t) \quad (5)$$

where Δt is the timestep. The sum in Eq.(5) is carried out only over the previous M steps, where $M\Delta t$ should be longer than the timescale over which the solute diffuses away. The equation of motion for the point chucker is then:

$$\mathbf{r}(t + \Delta t) = \mathbf{r}(t) + \frac{D_1}{k_B T} \Delta t \mathbf{f}(t) + \xi \quad (6)$$

where D_1 is the diffusion constant of the chucker and ξ represents Gaussian white noise with zero mean and variance $2D_1\Delta t$. Care is needed when selecting the parameters D_1 , D_2 and k_c for comparability of the results of the Langevin and MC simulations, because of the different time units of the two algorithms; however, dimensionless combinations of parameters can be defined which are equivalent between the two simulation schemes.

In our MC simulations, we expect that at high chucking rates, the solute particles will tend to form a cage around the chucker, restricting its diffusion. This effect is not included in the Langevin dynamics simulations where we consider a point chucker and a continuous solute field. The Langevin Dynamics simulations are therefore only valid for low chucking rates, where the solute concentration is small.

III. RESULTS

In Sections III A and III B, we first discuss the behaviour of a chucker in free space, with no external applied forces. We then determine the response of the chucker to a dragging

force in Section III C, and finally we discuss the behaviour of a chucker which sediments against an absorbing or hard-planar surface in Section III D.

A. Solute concentration profiles

We begin by investigating the concentration profile of solute particles around the chucker in our MC simulations when $R_1/R_2 = 10$, for a fixed chucker. Since the solute particles do not interact with each other, we expect the steady-state solute concentration profile to correspond to the solution of the diffusion equation (3), using the Green's function appropriate for a sink at distance L from the chucker. This solution (for the solute concentration c) is $c(r) = \frac{k_c}{4\pi D_2} \left(\frac{1}{r} - \frac{1}{L}\right)$, so that the solute volume fraction ϕ is given by $\phi(r) = \frac{k_c R_2^3}{3D_2} \left(\frac{1}{r} - \frac{1}{L}\right)$. We note that this is not a true volume fraction, since solute particles do not interact and can overlap in our model (so that ϕ can be greater than one); but it does give some indication of the density of the solutes, for comparison to real systems.

Figure 3 shows a comparison between the radial profiles for ϕ obtained from our simulations with the analytical expression, for $L = 4R_1$. The simulation data agrees very well with the analytical expression; the small discrepancy close to the boundary ($r/R_1 = 4$) occurs because the analytical expression is computed for a spherical boundary whereas the simulation has a cubic boundary.

We are also interested in how closely the solute particles are packed around the chucker: if the volume fraction close to the chucker surface is too high then the the Asakura-Oosawa approximation fails to accurately describe a real solute (e.g. polymer coils), since it neglects solute-solute interactions. Figure 4 shows the volume fraction ϕ of solute particles in spherical shells centred on the chucker in our MC simulations, computed for a freely diffusing chucker with $R_1/R_2 = 10$, over the full range of chucking rates used in our simulations ($0 < k_c R_2^2/D_1 \leq 600$). The maximum volume fraction obtained close to the chucker is about 0.12, and for most chucking rates it is much lower. This suggests that our neglect of solute-solute interactions is justified over the range of parameters used in this work.

B. Chucker diffusion

We now discuss the diffusive behaviour of an isolated chucker, using MC simulations with two different ratios of the chucker and solute radii: $R_1/R_2 = 10$ and $R_1/R_2 = 100$, for various chucking rates k_c . In our simulations, the solute particles are produced isotropically so there is no net directional motion. Rather, we observe diffusive behaviour, in which the mean square displacement $\langle r(t)^2 \rangle$ is linear in time. This allows us to compute an effective diffusion constant D_{eff} by linear fitting of the long-time behaviour of $\langle r(t)^2 \rangle$.

Figure 5 shows that in our simulations the effective diffusion constant D_{eff} of the chucker varies non-monotonically with the chucking rate k_c . Diffusive motion of the chucker is enhanced as the chucking rate increases, for low chucking rates. At high chucking rates, diffusive motion is inhibited due to crowding by the solute particles, so that D_{eff} decreases with k_c . We plot the dimensionless quantity D_{eff}/D_1 , where D_1 is the diffusion constant of the chucker for zero chucking rate, versus $k_c R_2^2/D_1$. The latter turns out to be the most relevant dimensionless parameter for comparison to theory: see Ref [11] and Eq.(7). R_2^2/D_1 is the typical time for the chucker to diffuse the radius of a solute particle; this ratio therefore measures the relative magnitudes of this time and the inverse of the chucking rate.

We believe that the mechanism behind the increase in D_{eff} with chucking rate, for small k_c , is as follows. A stationary chucker would be surrounded by a symmetric, concentration field of solute which decreases with distance from the chucker. A small random displacement of the chucker, however, positions it asymmetrically in the solute concentration field. Osmotic effects will then tend to cause the chucker to move further in the same direction, leading to a non-thermal osmotic enhancement of the effective diffusion constant of the chucker.

Comparing the results in Figure 5 for the two different ratios of chucker and solute radius, we find that the small k_c regime, where D_{eff}/D_1 increases with $k_c R_2^2/D_1$, appears not to depend strongly on the size of the solute – although the inset, plotted on a linear scale, suggests that the two plots do not actually collapse convincingly onto one curve. On the other hand, our data suggests that the regime, for large k_c , in which diffusion decays with chucking rate, does depend strongly on the size of the crowder: crowding effects kick in at smaller $k_c R_2^2/D_1$ for the smaller solute particles. This suggests that the dependence of the crowding effect on solute radius is less steep than $\sim R_2^2$.

Golestanian's recent theoretical work [11], which uses linearised hydrodynamics, predicts

that D_{eff}/D_1 should be given by:

$$\frac{D_{\text{eff}}}{D_1} = 1 + \left[1.17810 \left(\frac{\lambda}{R_1} \right)^4 \left(\frac{3}{\pi} \right) \right] \left(\frac{k_c R_2^2}{D_1} \right) \quad (7)$$

where we have substituted the Stokes-Einstein relation ($D_1 = \frac{k_B T}{6\pi R_1 \eta}$) and the relation $\mu = k_B T \lambda^2 / \eta$ into the expression given in Eq.(7) of Ref [11]. In our MC simulations, the imbalance of solute collisions across the chucker surface is expected to produce a net force which corresponds to a prefactor $A = (4/3)\pi R_1^3 k_B T$ in Eq.(2). This will produce a drift velocity $\mathbf{v} = \mathbf{f}/(6\pi\eta R_1)$. Linearized theory, which accounts for solvent-colloid surface interactions, predicts a colloid velocity $\mathbf{v}_s = -k_B T \lambda^2 \nabla c / \eta$ [11]. Matching these two relations, we find that our MC simulations have an effective λ value $\lambda = \sqrt{2} R_1 / 3$. Substituting this into Eq.(7), we obtain a prediction for D_{eff} in our MC simulations.

The inset to Figure 5 shows a comparison between this prediction and our MC data, for small chucking rates. For $R_1/R_2 = 100$, we obtain an excellent fit, whereas for the larger solute particles, $R_1/R_2 = 10$, the fit is much less convincing. We will revisit the effect of solute size in Figure 7. We note that Golestanian [11] also predicts a regime in which the mean square displacement $\langle r^2 \rangle$ is proportional to $t^{3/2}$, for timescales between the inertial and diffusive regimes, for an isotropic chucker. We do not observe this regime in our simulations: for ratios of $R_1/R_2 \geq 5$ the mean square displacement is linear in time.

To further investigate the relationship between chucker diffusion and solute concentration gradient, we performed additional MC simulations for a *passive* colloid, of radius R_1 , in a constant density gradient of Asakura-Oosawa solute particles (Fig.6). In order to maintain a constant density in steady state, we introduced a planar source of solute particles (of radius R_2) at the top of the simulation box, and a planar absorbing sink at the bottom. Solute particles are randomly seeded on the source plane at a constant rate k_c .

The analysis in Ref. [12] can be generalised to yield the following prediction for the steady state velocity of a colloidal particle in a constant concentration gradient (neglecting hydrodynamic effects):

$$v = \frac{4\pi R_2 R_1^2 k_c}{3L^2} \quad (8)$$

where the top and bottom planes have a surface area of L^2 , and we have again used the expectation that $\lambda = (\sqrt{2}/3)R_1$ in our simulations.

Figure 7 shows a comparison between the analytical prediction (8) and our simulation results, for $R_1/R_2 = 10$ (panel a) and $R_1/R_2 = 100$ (panel b). As in the inset to Figure 5,

the agreement with the theoretical prediction is much better for the smaller solute radius. This observation is not unexpected, given that the smaller solute radius is closer to the continuum limit. What is perhaps surprising is the extent of the deviation from the theory when $R_1/R_2 = 10$. For this solute radius, our simulation results deviate from the analytical prediction by about an order of magnitude.

An important drawback of our MC simulation scheme is that it does not account for the details of the solvent interactions with the chucker surface. As discussed in Section I, these effects may drastically reduce the magnitude of solute-induced effects on colloid mobility. In our MC simulations, an imbalance of solute concentration across the chucker surface leads to fewer overlaps (“collisions”) on one side of the chucker than the other, and hence net motion down the concentration gradient. We expect this to correspond to Eq.(2) with a prefactor of $A = (4/3)\pi R_1^3 k_B T$ (simply summing collisions across the colloid surface). We would expect hydrodynamic effects at the chucker surface (if included) to decrease this prefactor: for a solvent-impermeable chucker with no slip boundary conditions, linearised hydrodynamic theory predicts that the prefactor decreases by a factor $\sim \lambda^2/R_1^2$ where λ [the lengthscale for chucker-solute interactions] is $\sim R_2$ [11, 12, 28, 30]. If, on the other hand, the chucker is partially or totally permeable to solvent, the decrease in the prefactor due to these effects should be less severe [12, 27].

As discussed in Section II B, we can model the effects of solvent-chucker surface interactions approximately using Langevin dynamics simulations in which we vary the magnitude of the prefactor A : this corresponds to varying the hydrodynamic lengthscale λ . Figure 8 shows the effective diffusion constant D_{eff} , computed as a function of k_c using Langevin dynamics simulations with different prefactors, for $R_1/R_2 = 10$. The same qualitative behaviour is observed as in our MC simulations (compare to Figure 5): again, D_{eff}/D_1 increases with k_c for small chucking rates. For large chucking rates, the effective diffusion constant decreases in the MC simulations due to crowding effects which are not included in the Langevin Dynamics simulations

For small $k_c R_2^2/D_1$, we can make a quantitative comparison between the MC and Langevin simulation results, as shown in Figure 9. Here, the Langevin simulations were run with the “naive kinetic” prefactor $A = (4/3)\pi R_1^3 k_B T$. Excellent agreement is obtained between the two types of simulation. This reinforces our earlier conclusions that the MC simulations for small R_2 behave as would be predicted by hydrodynamic theory with a hydrodynamic

lengthscale $\lambda = (\sqrt{2}/3)R_1$.

C. A dragged chucker

For passive systems, such as colloidal particles, the fluctuation-dissipation theorem (FDT) states that the mobility coefficient Γ is fundamentally related to the diffusion constant D by $\Gamma = D/k_B T$. For active systems, there is no reason why the FDT should hold. Deviations from the FDT not only serve to demonstrate that the system is out of equilibrium, but can also yield insight into the underlying physics.

To investigate the relationship between mobility and diffusion for the colloidal chucker, we carried out MC simulations in which a chucker (with $R_1/R_2 = 10$) is dragged in a fixed direction by a constant force F (for example, using optical tweezers). We measure the velocity v of the chucker in the direction of the force. The mobility coefficient Γ is defined by $v = \Gamma F$; this can be compared with the value of D_{eff} obtained in Figure 5. In this work, we use values of F which approximately correspond to the magnitude of the gravitational force on a bacterium.

Figure 10 shows the steady state chucker velocity v , as a function of the chucking rate, expressed as the dimensionless ratio $k_c R_2^2/D_1$, for two different values of the pulling force F . This velocity depends strongly and nonmonotonically on the chucking rate, in a markedly different way to the effective diffusion constant of Figure 5.

Combining the results of Figures 5 and 10, we obtain Figure 11, which describes how the ratio $\Gamma k_B T/D_{\text{eff}}$ depends on $k_c R_2^2/D_1$. Deviation of $\Gamma k_B T/D_{\text{eff}}$ from unity (green dashed line) corresponds to violation of the FDT. We observe firstly that deviations from FDT in this system are strong (up to a factor of 3) and nonmonotonic. Depending on the chucking rate and the pulling force, mobility may dominate diffusion, or vice versa. As might be expected, the deviations from FDT are stronger for the larger pulling force. While it is not surprising that the FDT does not hold in this nonequilibrium system, what is perhaps unexpected is that the relationship between the mobility and diffusion constants has such a complex dependence on both the chucking rate and the applied force for this rather simple model.

The trends observed in Figure 11 can be tentatively related to changes in the solute configuration around the chucker, for different chucking rates and pulling forces. Naively, one

might imagine that for small chucking rates, where the density of solutes is low, the pulling force might tend to displace the chucker relative to its symmetric concentration gradient of solute, so that more solute would be behind it than in front, resulting in an osmotic enhancement of the mobility. This is what one would expect from an advection-diffusion equation with a source moving at a finite Peclet number (see e.g. Ref. [36]). However, for large chucking rates, the density of solutes near the chucker is higher, and one might imagine that the pulling force would lead to an increased collisions of the chucker with nearby solute particles, decreasing the mobility.

To test this hypothesis, we plot in Figure 12 the “volume fraction”, as defined by $\phi \equiv (4/3)\pi R_2^3 c$, of solute particles within the conical volume supported by the angle $\theta = \pi/9$, in front of and behind the chucker (the cone is extended all the way to the edge of the box). We first note that there is a difference in the volume fraction of solute in front of and behind the chucker, for large enough chucking rate. These effects are more pronounced for the larger pulling force. For $F = 7.0k_B T/R_1$, the solute concentration is larger behind than in front of the chucker, for chucking rates in the range $50 < k_c R_2^2/D_1 < 200$. We would expect this to cause an enhancement of mobility over diffusion; however, this range of k_c values is beyond the peak in $\Gamma k_B T/D_{\text{eff}}$ (as shown by the green dashed line). For higher chucking rates, we would expect to see a larger volume fraction in front of the chucker, if the solute particles are inhibiting chucker motility. There is some indication that this happens for the highest chucking rates (not shown in Figure 12). It is possible that this crowding effect plays a more important role for the smaller value of the force $F = 3.0k_B T/R_1$, where the pulling force is not strong enough to overcome the crowding; for the stronger pulling force $F = 7.0k_B T/R_1$, we speculate that the pulling force is strong enough to overcome this effect. Further work will be needed to fully understand the data in Figure 11; it is clear, however, that the nontrivial relationship between mobility and diffusion in this system is caused by a complex interplay between crowding and osmotic effects.

D. A sedimenting chucker

We now consider the case of a chucker which experiences a constant force F perpendicular to a planar surface which either absorbs the solute particles or behaves as a hard wall. This models the gravity-driven sedimentation of a chucker onto a surface, in the case where

gravitational effects on the solute particles are negligible. Although this model is highly simplified, the sedimentation of exopolysaccharide-producing bacteria onto surfaces is important in the formation of biofilms [37]. Here, the hard surface case might mimic the initial stages of biofilm formation, when bacteria sediment onto an uncolonised surface, while the absorbing surface might correspond to a situation where bacteria sediment onto an already formed biofilm which tends to absorb exopolysaccharide.

We determine the steady-state probability distribution function for the chucker position relative to the surface in our MC simulations. This would correspond to an experimental sedimentation density profile, in the case of low chucker density where interactions between chuckers can be ignored. In all our simulations, we take $R_1/R_2 = 10$, $F = 7.0k_B T/R_1$ and initialise the simulations with the centre of the colloid at a distance $z = 1.6R_1$ from the surface; we then begin to observe the system once a steady state has been reached (i.e. after 9×10^5 Monte Carlo cycles). This choice of F approximately corresponds to the gravitational force experienced by a typical bacterium.

Figure 13 shows the steady-state probability distribution $P(z)$ for the position of the centre of the chucker relative to the surface, which is at $z = 0$. In Figure 13(a), the wall acts as a sink for solute particles. This results in a buildup of the chucker probability density close to the surface: the higher the chucking rate, the more tightly the chucker tends to approach the surface. This effect can be understood in terms of an effective attractive interaction between the chucker and the surface, in which local depletion of solute near the surface causes an osmotic imbalance which squeezes the chucker against the surface. Figure 13(b) shows the corresponding probability density profiles when the planar surface instead acts as a hard wall. Here we find two regimes, depending on the chucking rate. For small chucking rates ($k_c R_2^2/D_1 \leq 1$), the probability density decreases monotonically away from the surface, with a steepness that decreases as k_c increases (for $k_c = 0$ we obtain a Boltzmann distribution). However, as k_c increases further, the profile develops a minimum close to the surface and a peak at some distance from the surface. This peak recedes from the surface with increasing k_c . For the hard surface, there is a solute-mediated osmotic repulsion between the chucker and the surface. The crossover between the two types of probability density profile occurs when this repulsion becomes strong enough to overcome the gravitational force pulling the chucker towards the surface. In the high k_c regime, the peak in $P(z)$ occurs where the gravitational and osmotic repulsion forces balance. We note

that for the hard wall, the solute density profile, and hence the steady-state chucker location, depends on the position of the absorbing box boundary, since a linear concentration gradient of solute arises between the colloid and the box boundary. However, the qualitative features of our results are independent of the boundary position.

IV. DISCUSSION

In this work, we have used computer simulations to study the physics of an active colloid (a “chucker”) of radius R_1 , which produces solute particles of radius R_2 isotropically on its surface, at a rate k_c . Most of our simulations have used a Monte Carlo scheme in which the chucker is modelled as a hard sphere and the solute particles as Asakura-Oosawa (*i.e.* mutually non-interacting) spheres. Our MC simulations were complemented by an overdamped Langevin dynamics approach in which the chucker is represented as a point particle which experiences a force proportional to the gradient of a concentration field of solute, this field being computed analytically using the Green’s function for free diffusion. The Langevin dynamics approach has the advantage that we can tune the prefactor that links the osmotic force to the solute concentration gradient: this provides a crude way to model hydrodynamic effects close to the chucker surface.

Our MC simulations of an isolated chucker in free space show diffusive behaviour, from which we extract an effective diffusion constant D_{eff} . This varies nonmonotonically with the chucking rate. For small values of k_c , solute chucking enhances diffusion. We interpret this as being due to the chucker being “pushed along” by a self-generated solute concentration gradient; the same behaviour is recovered in our Langevin dynamics simulations. An increase in D_{eff} as a function of k_c was recently predicted analytically by Golestanian [11]. In our MC simulations, when the chucking rate becomes large, the chucker tends to become caged by newly generated solute particles, hampering its diffusion. The result is therefore a peak in D_{eff} at intermediate chucking rate. In our simulations, the solute particles do not interact. For more realistic, interacting solutes, we might expect crowding to kick in at lower chucking rates, shifting the peak in D_{eff} towards smaller k_c .

A quantitative comparison between our MC simulation results and Golestanian’s theoretical prediction reveals that the simulations are in agreement with theory for a hydrodynamic length $\lambda = (\sqrt{2}/3)R_1$, for large values of the ratio between the sizes of the chucker and of the

solute particles, $R_1/R_2 = 100$; agreement is less convincing for $R_1/R_2 = 10$. This is the value of λ we would predict by matching the drift velocity predicted in a “naive” osmotic view, in which the colloid moves because of an imbalance in the number of solute collisions across its surface, with the colloid velocity, expressed as a function of λ , predicted by hydrodynamic theory. When we simulate a passive colloid in an externally imposed concentration gradient of solute particles, we also find good agreement with the hydrodynamic theory prediction with $\lambda = (\sqrt{2}/3)R_1$ for $R_1/R_2 = 100$, but for $R_1/R_2 = 10$, the diffusiophoretic mobility is smaller than might naively be predicted from osmotic pressure arguments. We speculate that this poor agreement for large solutes may be due to local fluctuations of the solute concentration field, neglected in the theory. We can also make a quantitative comparison, for small churning rates, between our MC and Langevin simulation results. For $R_1/R_2 = 100$, the two simulation schemes produce effective diffusion constants in good agreement, for a choice of Langevin prefactor of $A = (4/3)\pi R_1^3 k_B T$, corresponding to $\lambda = (\sqrt{2}/3)R_1$.

One of the initial motivations for this study was to investigate possible effects of exopolysaccharide production on bacterial diffusivity. The bacterium *X. campestris* produces xanthan polymer at a rate as high as 10^4 polymer coils per cell per second (as estimated from the data given in Refs. [18, 19]). Assuming a ratio $R_1/R_2 = 10 - 100$, corresponding to a polymer gyration radius of 10-100 nm, hence to a value of $k_c R_2^2/D_1 \sim 1 - 100$, and referring to Fig. 5, we find that the effective diffusion constant of the chucker should be significantly different from the infinite dilution value at this churning rate. On the other hand, the bacterium *Sinorhizobium meliloti*, a less prolific producer of exopolysaccharide, produces less than 1 polymer per bacterium per second [38], leading to a value of $k_c R_2^2/D_1$ of $10^{-4} - 10^{-2}$ (assuming the same dimensions for the polymer), so that for this bacterium, we expect the effect of polymer production on diffusion to be essentially perturbative. It would be interesting to compare the diffusion constants of mutants of *X. campestris* which are altered in their exopolysaccharide production rates: our simulations suggest a change in D_{eff} of up to about 50% if exopolysaccharide production were to be eliminated. One would need to be careful in such an experiment to avoid the buildup of polymer in the bacterial suspension, leading to crowding and a subsequent decrease in diffusion.

The chucker is an example of a nonequilibrium, “active” system, in which statistical mechanical relations such as the Fluctuation-Dissipation theorem (FDT) may not hold. Comparing the effective diffusion constant D_1 to a mobility coefficient computed by dragging

a chucker with a constant force in our MC simulations, we find that indeed this system violates the FDT strongly, in a highly nontrivial way. The complex relationship between mobility and diffusion in this system is due to an interplay between crowding and osmotic effects which depends sensitively on the applied force and chucking rate.

Finally, we have studied the behaviour of a chucker which sediments onto a planar surface which either absorbs the solute particles or behaves as a hard wall. When the surface is absorbing, a solute-mediated effective attraction (which increases with increasing k_c) pushes the chucker towards the surface. However, when we consider a hard surface, a solute-mediated effective repulsion exists. For small k_c this simply results in a decrease in the gradient of the chucker probability density profile near the surface. For large k_c , the repulsive interaction dominates the gravitational force near the surface, resulting in a peak in the probability density for the chucker position at some distance from the surface.

This work was motivated by recent experimental, theoretical and simulation work on colloidal “swimmers” which catalyse a chemical reaction, or secrete some product, anisotropically across their surface [8–15], by recent theoretical work on isotropic chuckers [11] and by the biological example of exopolysaccharide-secreting bacteria [16, 17]. However, the physical mechanisms explored here also have wider relevance in soft matter physics. As an example, Jiang *et al* [39] recently reported a system where migration of colloidal particles was mediated by inhomogeneities in polymer concentration, which were in turn induced by a temperature gradient. Dynamic depletion interactions between colloidal particles, in which one of the components of a phase separating binary fluid wets the colloid surface (creating a local depletion near the colloid), predicted in simulations by Araki and Tanaka [40], are also closely related to the phenomena studied here.

We hope that the results reported here will make a useful contribution to ongoing discussions concerning the effects of osmotic gradients on colloidal dynamics, as well as linking these discussions to the physics of biological systems (particularly exopolysaccharide-producing bacteria) and other nonequilibrium soft matter systems.

Acknowledgements: We thank M. E. Cates, O. Croze, G. Dorken, G. Ferguson, D. Frenkel, W. C. K. Poon, E. Sanz, P. Visco and L. Wilson for discussions and advice, and the referee for comments that have significantly improved the paper. This work was supported by EPSRC under grant EP/E030173/1. CV acknowledges support from a Marie Curie Fellowship. RJA was funded by the Royal Society of Edinburgh and by the Royal Society. This work has

made use of the resources provided by the Edinburgh Compute and Data Facility (ECDF). The ECDF is partially supported by the eDIKT initiative.

- [1] R.A.Simha and S.Ramaswamy, Phys.Rev.Lett. **89**, 058101 (2002).
- [2] V.Narayan, S.Ramaswamy, and N.Menon, Science **317**, 105 (2007).
- [3] Y.Hatwalne, S.Ramaswamy, M.Rao, and R.A.Simha, Phys.Rev.Lett. **92**, 118101 (2004).
- [4] I.Llopis and I.Pagonabarraga, Europhys.Lett. **75**, 999 (2006).
- [5] D.Marenduzzo, E.Orlandini, and J.M.Yeomans, Phys.Rev.Lett. **98**, 118102 (2007).
- [6] F.Schweitzer, in *Brownian Agents and Active Particles* (2003).
- [7] A.Sengupta, S. Teffelen, and H.Lowen, Phys.Rev.E **80**, 031122 (2009).
- [8] J.Howse and et al, Phys.Rev.Lett. **99**, 048102 (2007).
- [9] W.F.Paxton and et al, J.Am.Chem.Soc. **126**, 13424 (2004).
- [10] W.F.Paxton, A.Sen, and T.E.Mallouk, Chem.Eur.J. **11**, 6462 (2005).
- [11] R.Golestanian, Phys.Rev.Lett. **102**, 188305 (2009).
- [12] R.Golestanian, T.B.Liverpool, and A.Ajdari, Phys.Rev.Lett. **94**, 220801 (2005).
- [13] U.M.Cordova-Figueroa and J.F.Brady, Phys.Rev.Lett. **100**, 158303 (2008).
- [14] G.Ruckner and R.Kapral, Phys.Rev.Lett. **98**, 150603 (2007).
- [15] M.N.Popescu, S.Dietrich, and G.Oshanin, J.Chem.Phys. **130**, 194702 (2009).
- [16] I.W.Sutherland, Adv.Microb.Physiol. **23**, 79 (1982).
- [17] I.W.Sutherland, Biotechnology Advances **12**, 393 (1994).
- [18] H.Umashankar and et al, Bioprocess Engineering **14**, 307 (1996).
- [19] A.Prell, J.Lasik, J.Konicek, M.Sobotka, and J.Sys, Bioprocess Engineering **13**, 289 (1995).
- [20] J.Schwarz-Linek and et al, EuroPhysics Lett. **in press** (2010).
- [21] F.Jülicher and J.Prost, Phys.Rev.Lett. **103**, 079801 (2009).
- [22] A.Wysocki and H.Lowen, Phys.Rev.E **79**, 041408 (2009).
- [23] E.Sanz and D.Marenduzzo, J.Chem.Phys. **in press** (2010).
- [24] K. Kikuchi, M. Yoshida, T. Maekawa, and H. Watanabe, Chem. Phys. Lett. **185**, 335 (1991).
- [25] D. M. Heyes and A. C. Branka, Mol. Phys. **94**, 447 (1998).
- [26] A.Ajdari and L.Bocquet, Phys.Rev.Lett. **96**, 186102 (2006).
- [27] J.Nardi, R.Bruinsma, and E.Sackmann, Phys.Rev.Lett. **82**, 5168 (1999).

- [28] J.L.Anderson, Phys.Fluids **26**, 2871 (1983).
- [29] B.Chicocki and K.Hinsen, Physica A **166**, 473 (1990).
- [30] J.L.Anderson, Annu.Rev.Fluid Mech. **21**, 61 (1989).
- [31] S.Asakura and F.Oosawa, J.Chem.Phys **22**, 1255 (1954).
- [32] S.Asakura and F.Oosawa, J.Polym.Sci. **33**, 183 (1958).
- [33] A.Vrij, Pure Appl.Chem. **48**, 471 (1976).
- [34] M.P.Allen and D.J.Tildesley, in *Computer simulations of liquids* (1989).
- [35] R.Golestanian, T.B.Liverpool, and A.Ajdari, New J.Phys. **9**, 126 (2007).
- [36] C.A.Solari and et al, Proc.Nat.Acc.Science **103**, 1353 (2006).
- [37] I.W.Sutherland, Microbiology **147**, 3 (2001).
- [38] G.Dorken and L.Wilson (private communication).
- [39] H.-R.Jiang, H.Wada, N.Yoshinaga, and M.Sano, Phys.Rev.Lett. **102**, 208301 (2009).
- [40] T.Araki and H.Tanaka, J.Phys. : Condens.Matter **20**, 072101 (2008).

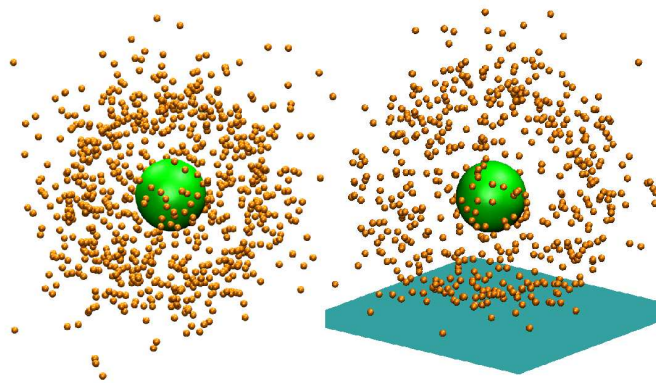


Figure 1: Snapshot of a freely diffusing chucker (left), and a chucker close to a hard-planar surface (right).

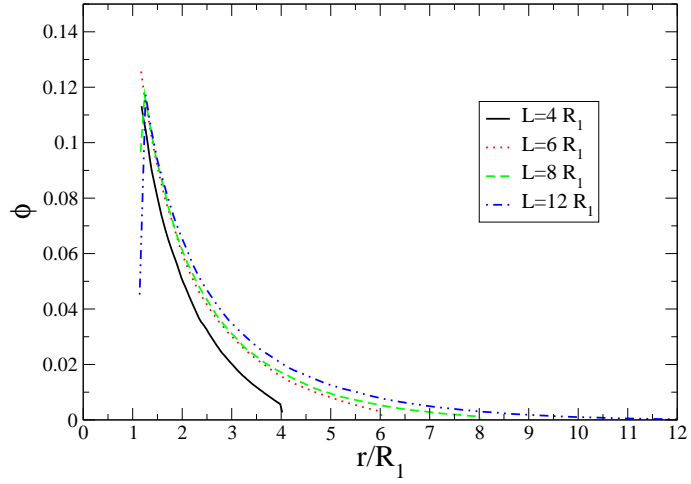


Figure 2: Volume fraction ($\phi \equiv (4/3)\pi R_2^3 c$ (where c is concentration)) of solute particles surrounding a motile-chucker ($R_1/R_2 = 10$) with $k_c R_1^2/D_2 = 600$ ($k_c = 0.001[MCcycles]^{-1}$) and various box size L .

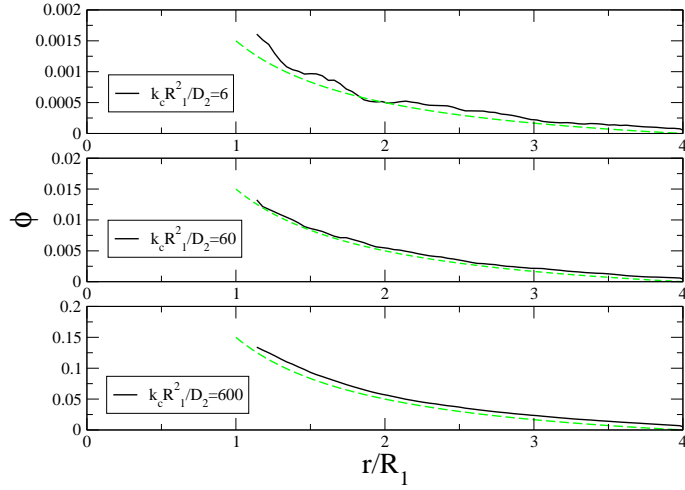


Figure 3: Comparison between analytical expression (green dashed-line) and simulated data (solid black line) for the “volume fraction” $\phi \equiv (4/3)\pi R_2^3 c$ (where c is concentration) of solute particles surrounding a non-motile chucker ($R_1/R_2 = 10$) with different values of k_c (from top to bottom, $k_c = 0.00001, 0.0001, 0.001$ [MC cycles] $^{-1}$). The corresponding values of the dimensionless ratio $k_c R_1^2/D_2$ are given in the legend, for comparison with the analytical expression. Note that since the solute particles can overlap, ϕ is not a true packing fraction.

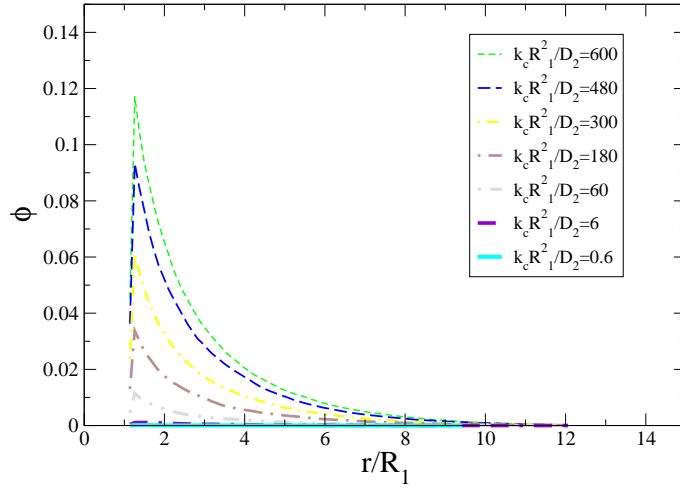


Figure 4: “Volume fraction” $\phi \equiv (4/3)\pi R_2^3 c$ (where c is concentration) of solute particles surrounding the chucker ($R_1/R_2 = 10$) as a function of the distance from the centre of the chucker (expressed in units of R_1). The corresponding values of the dimensionless ratio $k_c R_1^2 / D_2$ are given in the legend (note that the solute particles can overlap).

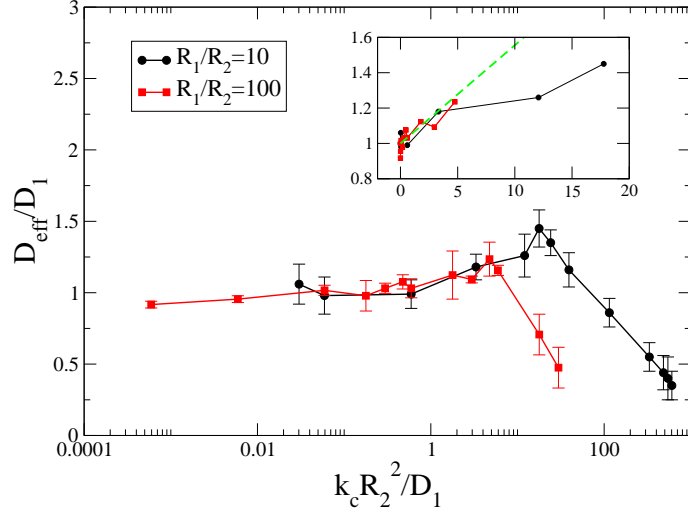


Figure 5: Effective diffusion coefficient D_{eff} of a chucker (normalised by the diffusion constant in the absence of chucking D_1) as a function of the dimensionless ratio $k_c R_2^2/D_1$, for $R_1/R_2 = 10$ (black circles) and $R_1/R_2 = 100$ (red squares). Note the logarithmic scale on the horizontal axis. The inset (on a linear scale) shows a comparison between the same data for small k_c and the theoretical prediction, Eq.(7), with $\lambda = \sqrt{2}R_1/3$ (green dashed line).

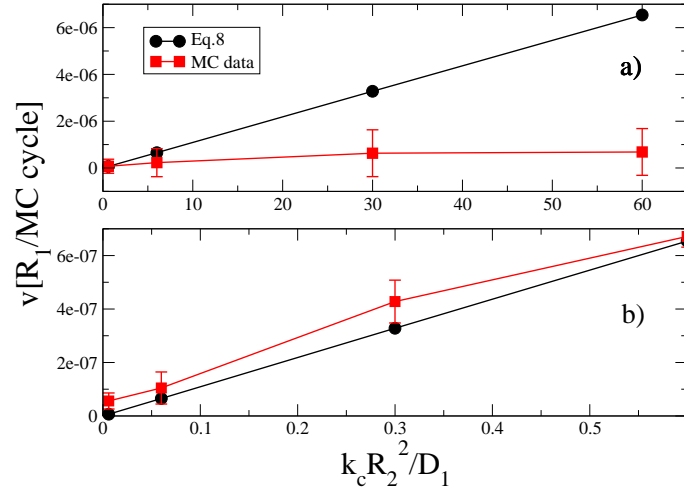


Figure 6: Snapshot of a passive colloid in a concentration gradient of Asakura-Oosawa solute particles: solute particles are generated at the top planar source, and removed at the bottom planar sink (the positions of these planes are indicated by the blue circles).

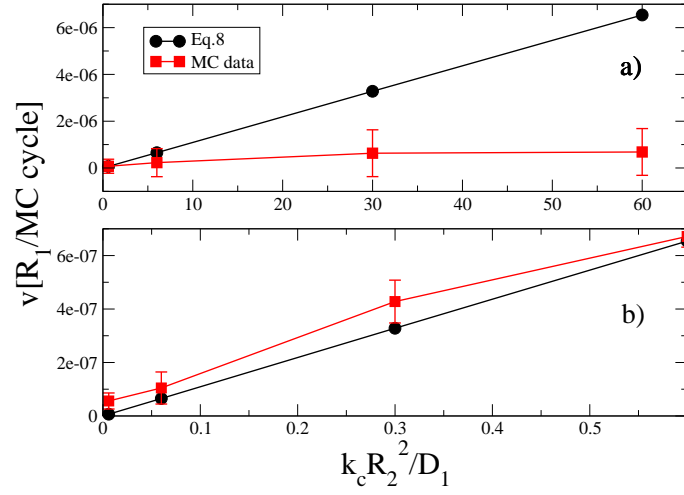


Figure 7: Sedimentation velocity for a passive colloid in a concentration gradient of solute, generated by a planar source and absorbed at a planar sink. The dimensionless combination $k_c R_2^2 / D_1$ measures the solute concentration gradient (note the colloid does not chunk in these simulations; solute is introduced into the simulation box at the source plane with rate k_c). The black circles indicate analytical results from Eq.(8), whereas the red squares are simulation data. (a): the case $R_1/R_2 = 10$ (b): the case $R_1/R_2 = 100$.

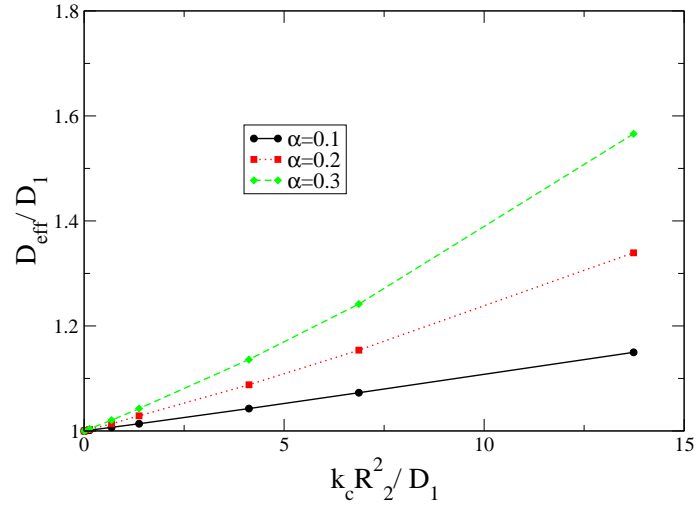


Figure 8: D_{eff} computed with Langevin dynamics simulations. The Langevin dynamics simulations are performed with various prefactors $A = \alpha k_B T R_1^3$, where $k_B T = 1$, and the values of α are given in the legend.

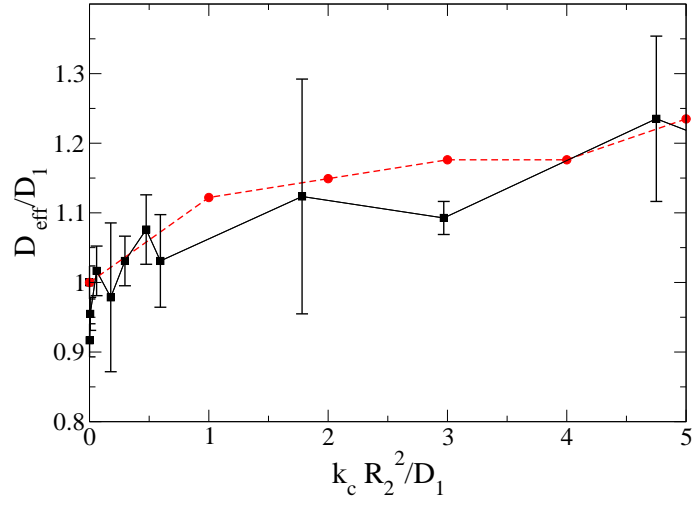


Figure 9: D_{eff}/D_1 versus the dimensionless ratio $k_c R_2^2/D_1$ for a chucker with $R_1/R_2 = 100$: the black continuous line represents the MC data and the red dashed line the Langevin results with $A = (4/3)\pi R_1^3 k_B T$. The plot shows data only for small values of $k_c R_2^2/D_1$.

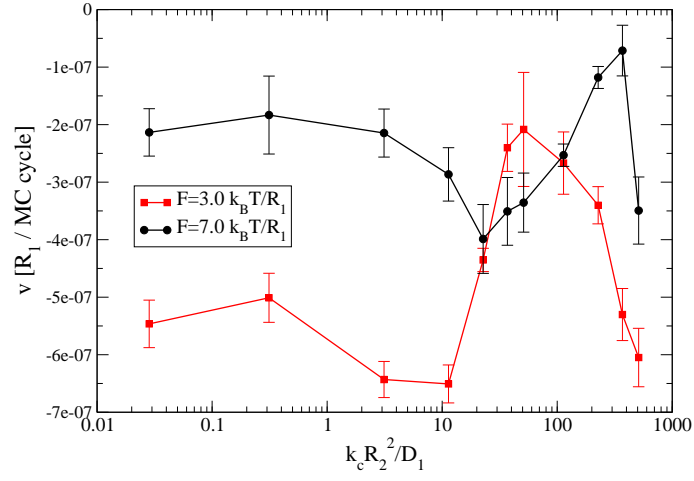


Figure 10: Asymptotic velocity v versus the dimensionless ratio $k_c R_2^2 / D_1$ for a chucker under an external force of $F = 3.0 k_B T / R_1$ or $F = 7.0 k_B T / R_1$ ($R_1 / R_2 = 10$).

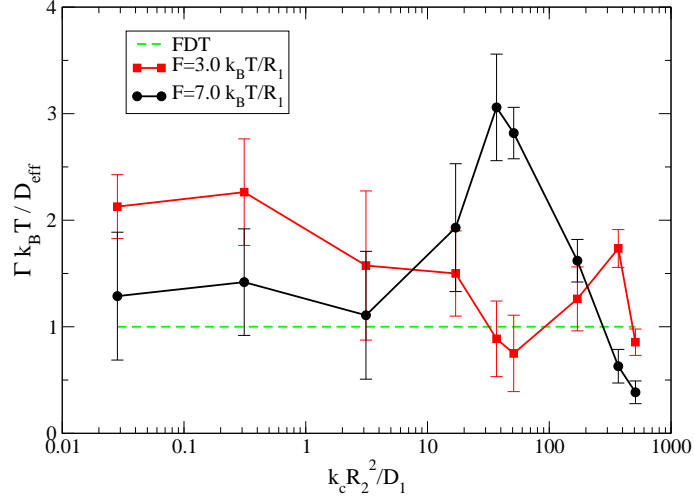


Figure 11: $\frac{\Gamma k_B T}{D_{\text{eff}}}$ versus the dimensionless ratio $k_c R_2^2 / D_1$, for a chucker with $R_1 / R_2 = 10$. D_{eff} is measured from the mean square displacement of a freely diffusing chucker (Figure 5) whereas Γ is obtained by dragging the chucker with an external force of $F = 3.0 k_B T / R_1$ or $F = 7.0 k_B T / R_1$ (Figure 10). The dashed line indicates the FDT prediction for a passive system.

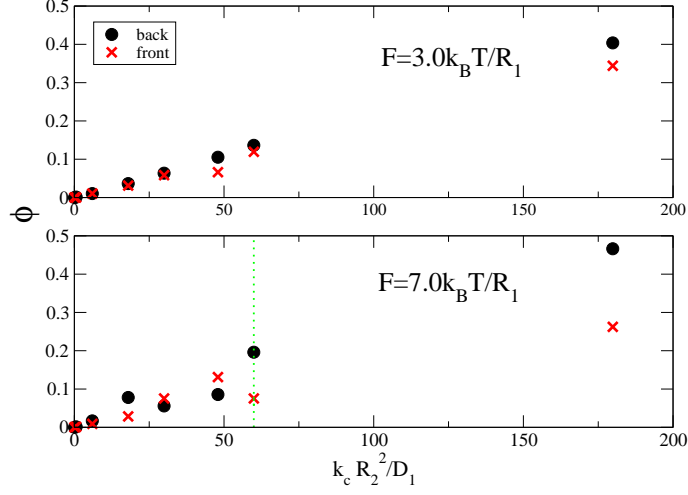


Figure 12: “Volume fraction” $\phi \equiv (4/3)\pi R_2^3 c$ (where c is concentration) of solute within a cone of angle $\theta = \pi/9$ at the front (red crosses) and at the back (black dots) of the pulled chucker, as a function of the dimensionless ratio $k_c R_2^2/D_1$, for a chucker with $R_1/R_2 = 10$ pulled by an external force of $F = 3.0k_B T/R_1$ or $F = 7.0k_B T/R_1$. The green dotted line represents the position of the peak of $\Gamma k_B T/D_{\text{eff}}$ in Figure 11. For $F = 3.0k_B T/R_1$, the peak of $\Gamma k_B T/D_{\text{eff}}$ is around 360 and not shown. Note also that the solute particles can overlap.

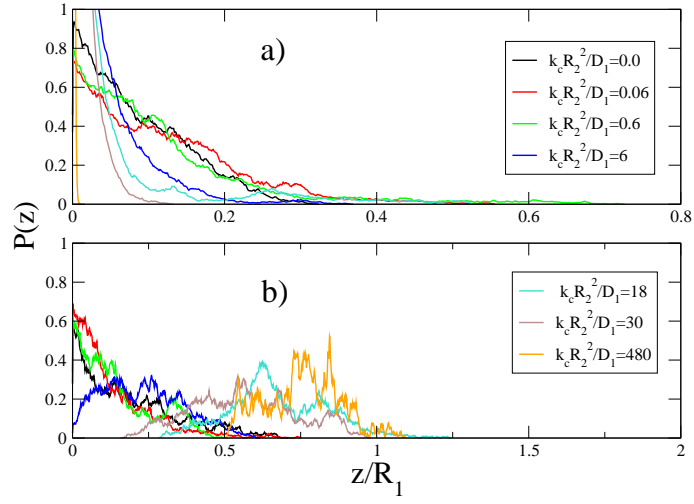


Figure 13: Steady-state probability distribution for the z -coordinate of the centre of the sedimenting chucker, for $R_1/R_2 = 10$ and various chucking rates (indicated in the legend).